ARL-TR-9064 ● SEP 2020

DEVCOM ARMY RESEARCH LABORATORY

Spectroscopic Investigation of Dysprosium-Doped Barium Fluoride (BaF_2) Single Crystals Relevant to the 3-µm Mid-IR Transition

by Zackery Fleischman, Jenny Rosen, Ei Ei Brown, and Mark Dubinskii

NOTICES

Disclaimers

The findings in this report are not to be construed as an official Department of the Army position unless so designated by other authorized documents.

Citation of manufacturer's or trade names does not constitute an official endorsement or approval of the use thereof.

Destroy this report when it is no longer needed. Do not return it to the originator.

ARL-TR-9064 ● SEP 2020

Spectroscopic Investigation of Dysprosium-Doped Barium Fluoride (BaF_2) Single Crystals Relevant to the 3-µm Mid-IR Transition

Zackery Fleischman, Ei Ei Brown, and Mark Dubinskii
Sensors and Electron Devices Directorate, CCDC Army Research Laboratory

Jenny Rosen
Cornell University

REPORT DOCUMENTATION PAGE

Form Approved
OMB No. 0704-0188

1. REPORT DATE *(DD-MM-YYYY)*	2. REPORT TYPE	3. DATES COVERED (From - To)
September 2020	Technical Report	1 June 2019–30 August 2020

4. TITLE AND SUBTITLE

Spectroscopic Investigation of Dysprosium-Doped Barium Fluoride (BaF_2) Single Crystals Relevant to the 3-µm Mid-IR Transition

5a. CONTRACT NUMBER

5b. GRANT NUMBER

5c. PROGRAM ELEMENT NUMBER

6. AUTHOR(S)

Zackery Fleischman, Jenny Rosen, Ei Ei Brown, and Mark Dubinskii

5d. PROJECT NUMBER

5e. TASK NUMBER

5f. WORK UNIT NUMBER

7. PERFORMING ORGANIZATION NAME(S) AND ADDRESS(ES)

CCDC Army Research Laboratory
ATTN: FCDD-RLS-RL
2800 Powder Mill Road
Adelphi, MD 20783-1138

8. PERFORMING ORGANIZATION REPORT NUMBER

ARL-TR-9064

9. SPONSORING/MONITORING AGENCY NAME(S) AND ADDRESS(ES)

10. SPONSOR/MONITOR'S ACRONYM(S)

11. SPONSOR/MONITOR'S REPORT NUMBER(S)

12. DISTRIBUTION/AVAILABILITY STATEMENT

Approved for public release; distribution is unlimited.

13. SUPPLEMENTARY NOTES

14. ABSTRACT

In the pursuit of new mid-IR laser gain materials, dysprosium-doped barium fluoride was evaluated for its potential laser emission in the 3.0-µm spectral region. Comprehensive spectroscopic characterization was performed, including absorption, fluorescence, and decay-time measurements. Laser-relevant parameters such as absorption and stimulated-emission cross sections, quantum-efficiencies, and radiative lifetimes were determined for room temperature (300 K) and cryogenic temperature (77 K). The gain cross sections, which predict overall laser performance, were also calculated.

15. SUBJECT TERMS

spectroscopy, laser, rare-earth, dysprosium, fluorides, crystals

16. SECURITY CLASSIFICATION OF:			17. LIMITATION OF ABSTRACT	18. NUMBER OF PAGES	19a. NAME OF RESPONSIBLE PERSON
a. REPORT	b. ABSTRACT	c. THIS PAGE			Zackery Fleischman
Unclassified	Unclassified	Unclassified	UU	22	19b. TELEPHONE NUMBER (Include area code) (301) 394-1142

Contents

List of Figures

List of Tables

1. Introduction

Laser development in the mid-IR spectral region (2–5 μm) has been of particular interest recently due to a wide range of potential applications. In particular, lasers operating between 2.5 and 3 μm can take advantage of the strong absorption by water and OH-radicals in that region (Fig. 1) to be instrumental in such applications as remote atmospheric sensing,[1] medical procedures,[2] and wind lidar.[3] Such lasers can also find utility in molecular spectroscopy and the pumping of longer-wavelength solid-state lasers. A significant amount of the ongoing mid-IR laser research is focused on rare-earth (RE)-doped materials, because RE active ions can provide a number of favorable energy transitions in the desired wavelength range.[4–6] Among the various RE ions, erbium (Er^{3+}) and holmium (Ho^{3+}) have been studied extensively for their transitions in the 2.5- to 3-μm spectral region.[7,8] However, in recent years dysprosium (Dy^{3+}) has received increased interest for its $^6H_{13/2} \rightarrow {}^6H_{15/2}$ transition, which produces approximately 3-μm emission.[9,10]

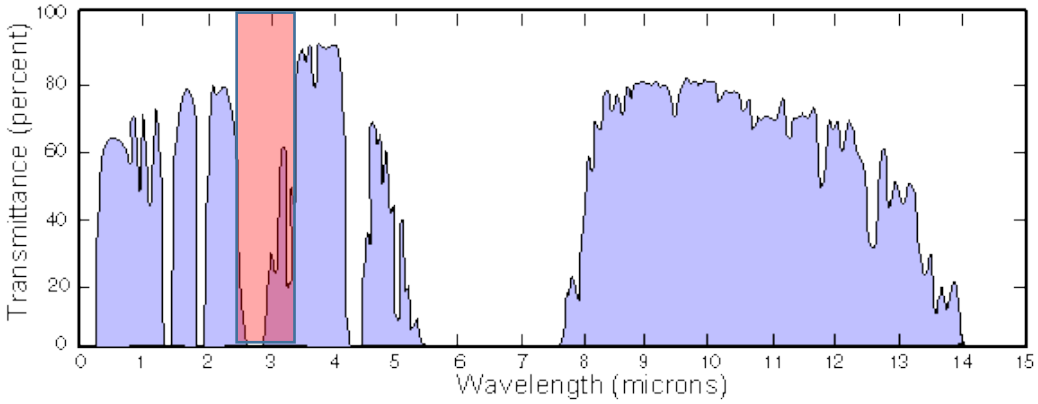

Fig. 1 Transmission spectrum of the atmosphere. Highlighted section is mid-IR area of interest.

Complications in the development of mid-IR lasers arise because the relatively small energy gaps needed to generate mid-IR photons are especially susceptible to nonradiative decay mechanisms such as multiphonon relaxation (MPR). To achieve higher emission efficiencies, the RE dopants must be hosted by materials with low maximum phonon energies to mitigate these MPR processes.[11,12] Fluorites (calcium fluoride [CaF_2], strontium fluoride [SrF_2], and barium fluoride [BaF_2]) have emerged as interesting host crystals due to their low phonon energies, high thermal conductivities, and ability to incorporate RE dopants.[9,13,14] Dy^{3+} has been studied in CaF_2[15] and SrF_2,[16] but its spectroscopic properties are largely unexplored in BaF_2.

In this work, we present a spectroscopic investigation of the 2.8-μm mid-IR emission properties of Dy^{3+}:BaF_2. Results of absorption and fluorescence measurements were used to generate stimulated-emission cross sections, and the gain characteristics were determined at both room temperature and 77 K.

2. Experimental Details

2.1 BaF_2 Sample Information

BaF_2 has a cubic crystal structure with a space group symmetry of Fm3m and a density of 4.89 g/cm^3. Its transmission window extends from 0.2 to 14 μm due to its large bandwidth of 11 eV.[17] The maximum phonon energy has been quoted in literature to be 319 cm^{-1};[18] however, our measurements show the main peak to be at 240 cm^{-1} with a very weak shoulder at 385 cm^{-1}, as shown in Fig. 2. RE-dopant ions are assumed to be incorporated into the divalent Ba^{2+} lattice sites, requiring a charge compensation mechanism. It was reported that for RE-doped into fluorites, the charge is compensated by an interstitial fluorine ion at the nearest neighbor position of C_{4v} symmetry.[17]

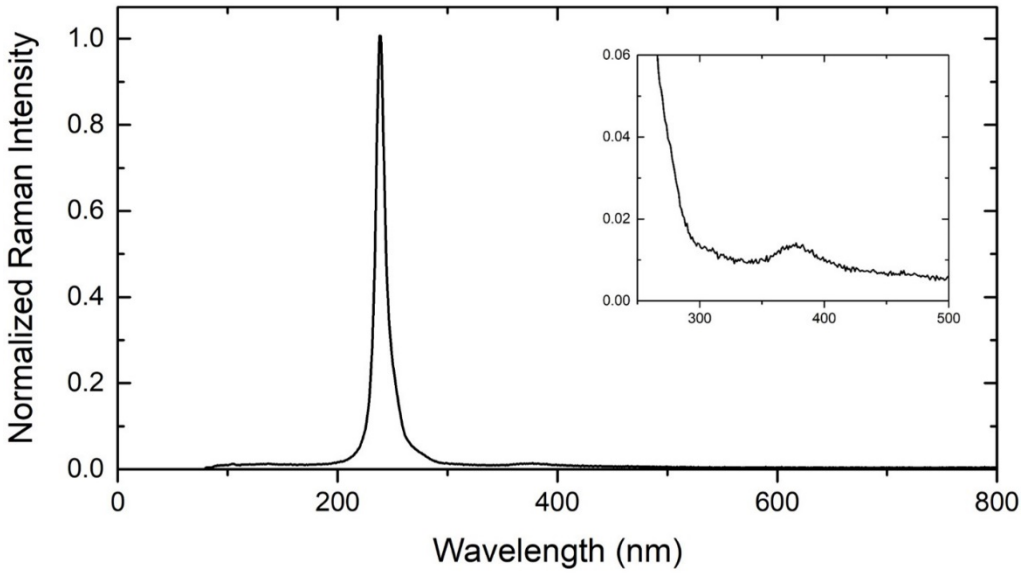

Fig. 2 Raman spectrum of BaF_2

The Dy^{3+}-doped BaF_2 single crystals studied in this work were grown by Bridgman technique with RE concentrations of nominally 1 and 2 at.% corresponding to 1.67×10^{20} ions/cm^3 and 3.35×10^{20} ions/cm^3, respectively. Samples arrived in the form of an as-grown boule and were diced and polished prior to spectroscopic characterization. Figure 3 depicts samples in various stages of this preparation.

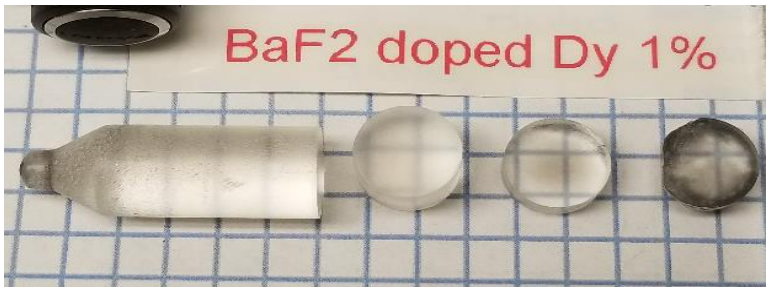

Fig. 3 Dy^{3+}:BaF_2 samples in various stages of being cut and polished

2.2 Spectroscopic Measurements

Room-temperature absorption spectra were recorded using a Cary 6000i spectrophotometer for the region from 600–1700 nm and a Nicolet 6700 Fourier-transform IR spectrometer for wavelengths greater than 1700 nm. All mid-IR fluorescence spectra were excited at 898.7 nm by a continuous-wave Spectra-Physics Tsunami titanium (Ti):sapphire laser tunable in the wavelength range from 800 to 990 nm. Mid-IR fluorescence spectra were collected using a Horiba Fluorolog-3 system with an iHR-320 monochromator (λ_{blaze}: 2 μm, 300 grooves/mm), and the emission signal was recorded by an Infrared Associates liquid-nitrogen-cooled InSb detector in conjunction with a Stanford Research Systems SR830 dual-phase lock-in amplifier. Fluorescence decay measurements were carried out using the output of a pulsed (10-ns pulses, 10 Hz) neodymium:yttrium aluminum garnet (Nd:YAG)-pumped Optical Parametric Oscillator system. The decay signal was recorded with a homemade labview program using a National Instruments data acquisition system. For temperature-dependent emission studies down to 10 K, the sample was mounted on the cold finger of a two-stage closed-cycle helium refrigerator.

Measurements of the Raman spectrum were recorded using a Renishaw Raman microscope equipped with three excitation sources at 514, 633, and 785 nm.

3. Results and Discussion

The Dy^{3+} ion offers a number of possible transitions in the near- and mid-IR, as shown by the energy level diagram in Fig. 4. For spectroscopic characterization of the approximately 2.8-µm mid-IR transition of Dy^{3+}:BaF_2, only the two lowest manifolds of the dysprosium ion are relevant. This study involved absorption measurements from the ground state ($^6H_{15/2}$) to the $^6H_{13/2}$ excited manifold, fluorescence lifetime measurements of this excited state, and measurements of the fluorescence spectrum for the $^6H_{13/2} \rightarrow {}^6H_{15/2}$ transition. These basic measurements, performed over a wide range of temperatures, provide laser-relevant information on the quantum efficiency, the stimulated-emission cross section, and the gain cross section for the 2.8-µm transition.

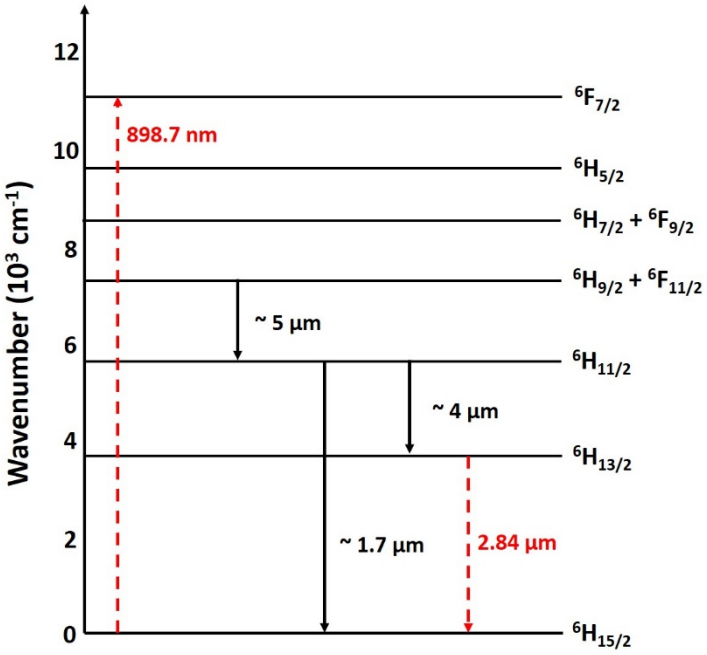

Fig. 4 Energy level diagram of Dy3+ with various near-and mid-IR transitions noted. The 2.8-µm mid-IR transition of interest and the fluorescence excitation transition (898.7 nm) are highlighted.

3.1 Absorption Measurements

Initial absorption measurements of the 1-at.% Dy^{3+}:BaF_2 sample were conducted at room temperature across a wide spectral range from 600 to 3300 nm. These results, shown in Fig. 5, provide important information on the absorption band of interest ($^6H_{13/2}$) as well as a number of other absorption lines in the near-IR that could be used for excitation purposes. Of particular interest are the absorption peaks in the 800- to 1000-nm region because those could be pumped by commercial diode or

Ti-sapphire lasers. In fact, the absorption line associated with the $^6H_{15/2} \rightarrow {}^6F_{7/2}$ transition at 898 nm served as the excitation pathway during our fluorescence spectroscopy measurements.

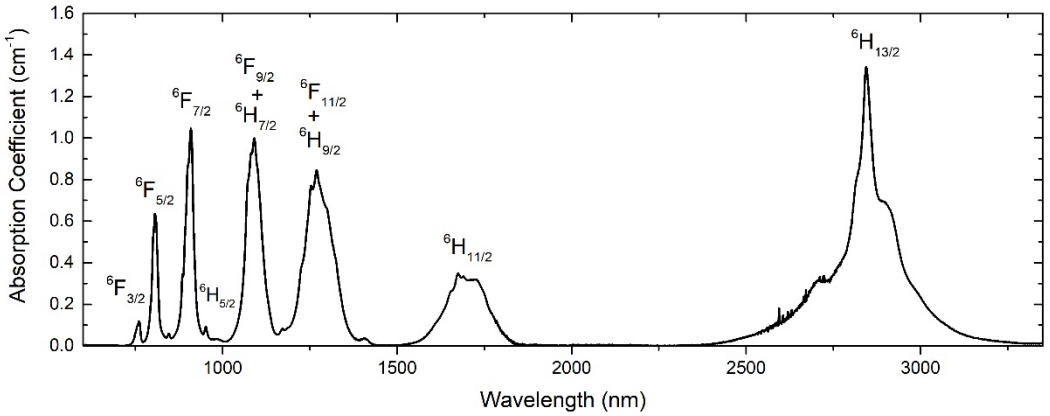

Fig. 5 Room temperature absorption coefficient of Dy^{3+}:BaF_2

High-resolution ground-state absorption spectra into the $^6H_{13/2}$ manifold were measured at several temperatures in the range of 10–300 K for the 2-at.% Dy^{3+}:BaF_2 sample. Absorption cross sections were calculated from the 300-K (room temperature) and 77-K (cryogenic temperature) absorption data using Beer's law and the RE-dopant concentration of 3.35×10^{20} ions/cm^3. Figure 6 shows that the highest absorption peak (~2842 nm) grows by a factor of 4 when cooling the sample from room temperature to 77 K, with peak intensities of 0.4×10^{-20} cm^2 and 1.6×10^{-20} cm^2, respectively.

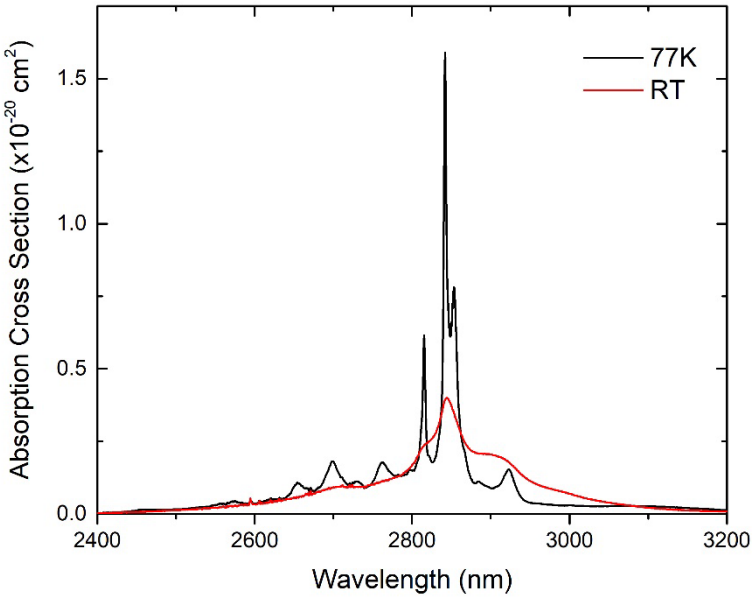

Fig. 6 Absorption cross section of the first excited state for 2-at.% Dy^{3+}:BaF_2 at 300 K (red) and 77 K (black)

3.2 Energy Level Analysis

Detailed information on the energy levels relevant to the 2.8-μm transition is imperative for determining the stimulated emission cross section using the McCumber method, which exploits the reciprocal nature of the absorption and stimulated emission transitions. This reciprocity relation is written

$$\sigma_{se}(\lambda) = \sigma_{abs}(\lambda)\frac{Z_L}{Z_U} exp\left[\frac{E_{ZL} - {}^{hc}/_{n\lambda}}{k_B T}\right] \quad (1)$$

where $\sigma_{se}(\lambda)$ and $\sigma_{abs}(\lambda)$ are the respective stimulated emissions and absorption cross sections as a function of wavelength λ; Z_L and Z_U are the partition functions for the lower and upper manifold, respectively; E_{ZL} is the "zero line" energy between the lowest levels of the two manifolds; h is Planck's constant; c is the speed of light in vacuum; n is the refractive index of air, in which the wavelength is measured; k_B is Boltzmann's constant; and T is the temperature. Among all these terms, the zero line energy and the partition functions are the ones that require knowledge of the exact positioning of all levels in respective upper and lower manifolds.

Taking into account that the static BaF_2 crystal field experienced by the dysprosium ion should split its manifolds into 2J+1 Stark levels, and also factoring in the Kramers degeneracy rule, we should expect the $^6H_{15/2}$ manifold to have eight levels and the $^6H_{13/2}$ manifolds to have seven levels. To determine these energy levels, we typically record numerous absorption and emission spectra and observe how the spectral peaks change as a function of temperature. At the lowest sample temperatures, the spectrum should be dominated by transitions originating from the lowest energy level of the initial manifold. As the sample temperature is increased, transitions from thermally excited levels (i.e., "hot lines") of the initial manifold grow in intensity.

Figure 7a shows absorption spectra to the first excited state of Dy^{3+} for a number of sample temperatures down to 15 K. While the spectral lines do get significantly narrower at the lower temperatures, they are still much too wide to allow for non-arbitrary energy level assignments. Additionally, even at the lowest temperature, there are many more than the expected seven spectral peaks that present themselves as coming from the lowest level of the ground manifold. To look at a simpler manifold, a similar series of measurements was performed for absorption into the $^6F_{3/2}$ level at approximately 750 nm, where there should only be two dominant peaks at the lowest temperature. The results, shown in Fig. 7b, display eight distinct peaks all presenting the opposite behavior from what would be expected for "hot lines", namely an increasing relative intensity with increasing temperature. While the $^6F_{3/2}$ absorption results also proved too difficult to allow for

energy level assignments, they do imply that there may be multiple Dy^{3+} incorporation sites in our material. Such a conclusion is not unwarranted considering there is a charge mismatch between the RE dopant and its substitutional counterpart Ba^{2+}, which could lead to all kinds of distortions of the crystal lattice.[17]

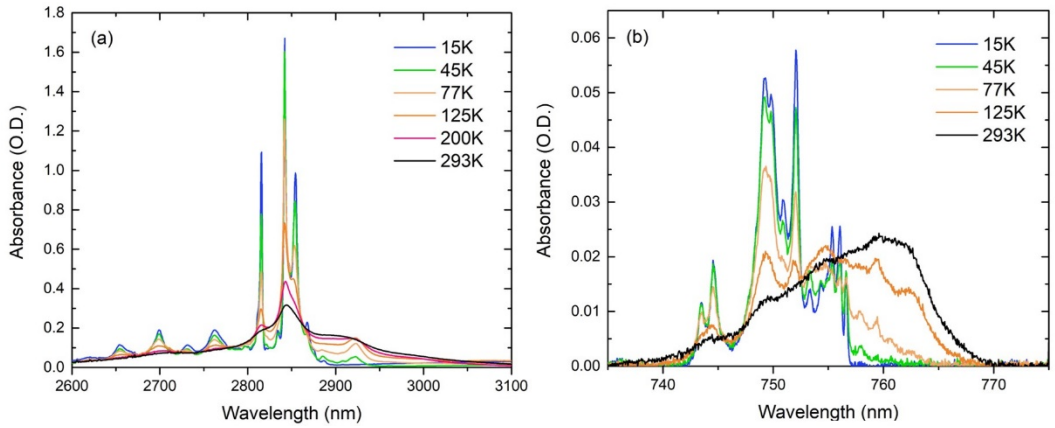

Fig. 7 Absorption spectra from the ground state into the a) $^6H_{13/2}$ and b) $^6F_{3/2}$ manifolds as a function of temperature for Dy^{3+}:BaF_2

Since analysis of the low-temperature absorption spectra proved fruitless in the determination of the Dy^{3+} energy levels, an alternative approach was necessary. The work of Zhang et al.[19] describes a method for estimating E_{ZL} and the Z_L/Z_U ratio that does not require knowledge of the discrete level energies. Instead, all that is needed is a comparison between absorption and fluorescence spectra. In practice, these two spectra are separately normalized and then plotted on the same graph as a function of energy. According to the reciprocal principle, the cross point of the spectra should be the zero line E_{ZL}. Measuring the low energy width of the fluorescence spectrum, from E_{ZL}, gives information about the energy spacing of the lower manifold, while similarly measuring the high energy width of the absorption spectrum gives information about the energy spacing of the upper manifold. Assuming the levels of each manifold are equally spaced, Z_L/Z_U can be estimated to be the ratio of the low energy width to the high energy width. Because the baselines between the two spectra can be ambiguous, the energy widths are determined for the point where the spectral intensity drops below 5% of the peak intensity.

The plots in Figure 8a and 8b depict the normalized Dy^{3+}:BaF_2 absorption and fluorescence spectra used to determine E_{ZL} and Z_L/Z_U for room temperature (300 K) and cryogenic temperature (77 K), respectively. These parameters for both temperatures are presented in Table 1. Note that Z_L/Z_U for the 300 K data is very close in value to the ratio $8/7 \approx 1.14$ we would get from simply dividing the number of upper-manifold Stark levels by the number of lower-manifold Stark levels. The

overall smaller energy widths observed in the 77 K results are attributed to less-thermal population of higher-lying levels in the upper and lower manifolds.

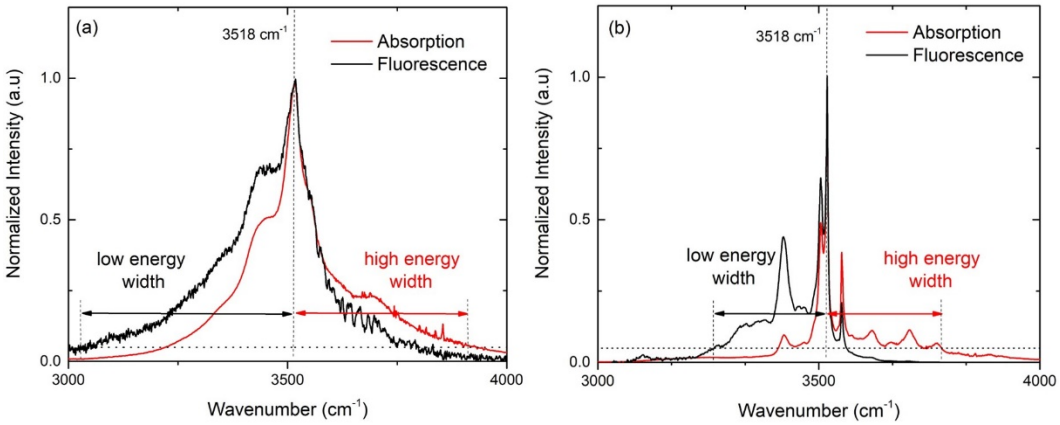

Fig. 8 Normalized absorption and fluorescence spectra for Dy^{3+}:BaF_2 at a) 300 K and b) 77 K

Table 1 Parameters related to energy level determination in Dy^{3+}:BaF_2

Temperature (K)	Zero line E_{ZL} (cm^{-1})	Low-energy width (cm^{-1})	High-energy width (cm^{-1})	Z_L/Z_U
300	3518	464	414	1.12
77	3518	269	265	1.01

3.3 Fluorescence Lifetimes

The fluorescence lifetime of Dy^{3+}:BaF_2 was measured by exciting the $^6H_{11/2}$ manifold using a pulsed 1723-nm laser. After subsequent de-excitation, the decay transient of the $^6H_{13/2}$ manifold of Dy^{3+} was measured for a number of temperatures between 77 K and room temperature. For all temperatures, the decay waveforms exhibited single exponential behavior, shown in Fig. 9a. The lifetime trend as a function of temperature is shown in Fig. 9b, exhibiting an increase from 1.5 ms at room temperature to 5.3 ms at 77 K. Additionally, while at high temperatures, the lifetime increases linearly with temperature, there is an apparent leveling off as the sample drops below 125 K. This behavior implies that nonradiative phonon decay is competing with the fluorescence at high temperatures, but this process decreases as phonons are frozen out at the lowest temperatures. These results compare very well with those seen for Dy^{3+}-doped BaY_2F_8, which has a reported maximum phonon energy of 350 cm^{-1}.[20]

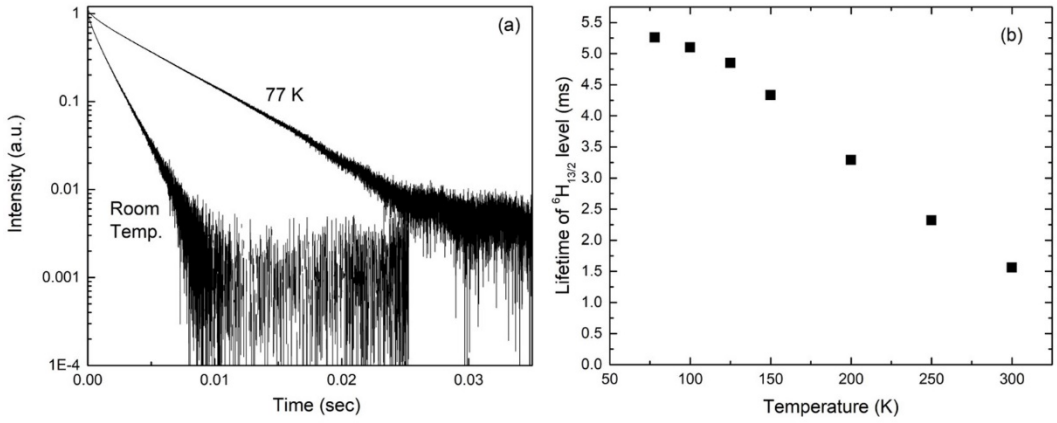

Fig. 9 a) Fluorescence decay transient of the $^6H_{13/2}$ manifold of Dy^{3+}:BaF_2 for room temperature and 77 K, and b) fluorescence lifetime values as a function of temperature

3.4 Stimulated Emission Cross Sections

Stimulated emission cross sections were obtained using a combination of the McCumber and Fuchtbauer–Ladenburg (F–L) methods. The McCumber method uses the reciprocity relation shown in Eq. 1 to calculate the stimulated emission cross section from the absorption cross section and the energy-level-related parameters given in Table 1. The stimulated emission cross section can also be calculated from the fluorescence and lifetime data using the F–L equation[21]:

$$\sigma_{se}(\lambda) = \frac{\eta\lambda^5}{8\pi c n^2 \tau_f} \frac{I(\lambda)}{\int I(\lambda)\lambda d\lambda} \tag{2}$$

where η is the quantum efficiency of the transition, $I(\lambda)$ is the fluorescence intensity at wavelength λ, n is the index of refraction of the RE host crystal (BaF_2), and τ_f is the measured fluorescence lifetime. In general, there is a branching ratio term in the numerator of Eq. 2; however, for transitions between the first excited manifold and the ground manifold, the branching ratio is unity and can be omitted.

By themselves, the reciprocity equation and the F–L equation are often inadequate to obtain a complete and accurate stimulated emission cross section. The reciprocity solution, while accurate at shorter wavelengths, tends to blow up at wavelengths longer than the zero line due to the exponential factor in Eq. 1. And the F–L equation easily provides the correct spectral shape of the cross section, but hard-to-measure quantities like the quantum efficiency make determining the correct scale difficult. For these reasons, the stimulated emission cross sections in this work were obtained by scaling the F–L data to match the reciprocity results in the short wavelength region and then stitching together the data sets at a convenient crossover point.

The stimulated emission cross sections of Dy^{3+}:BaF_2 for room temperature and 77 K are shown in Fig. 10. At room temperature, the highest intensity peak occurs at 2847 nm with a value of 4.5×10^{-21} cm^2. Cooling to room temperature shows a nearly 4× increase in the peak cross section, with a value of 1.58×10^{-20} cm^2 as well as a 7× decrease in the spectral line width.

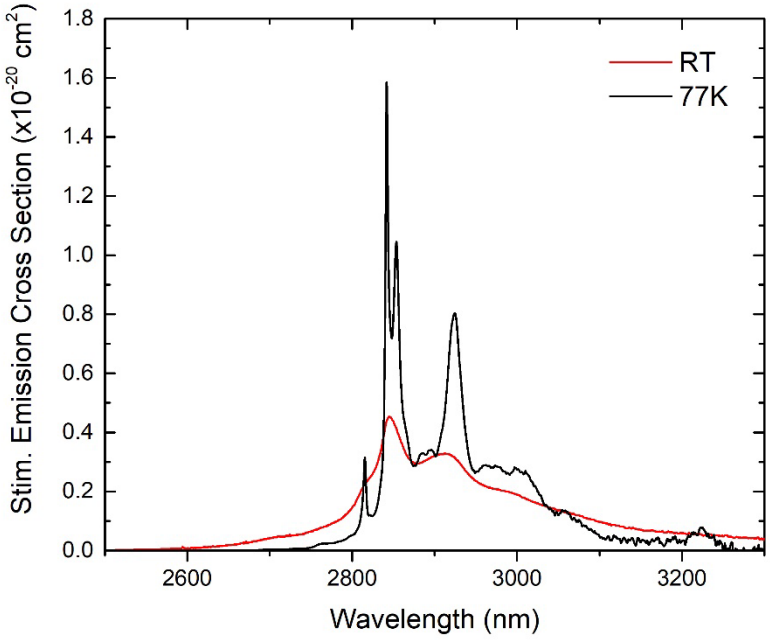

Fig. 10 Stimulated emission cross sections for Dy^{3+}:BaF_2 at room temperature and 77 K

3.5 Radiative Lifetime and Quantum Efficiency

Once an accurate stimulated emission cross section is obtained, the F–L equation can be rearranged to calculate for the quantum efficiency η and then the radiative lifetime τ_{rad} can be determined from the following relationship:

$$\eta = \frac{\tau_{fl}}{\tau_{rad}} \tag{3}$$

The values for both the measured fluorescence lifetime and calculated radiative lifetime of the $^6H_{13/2}$ manifold, as well as the quantum efficiency of the transition to the ground state, are presented in Table 2 for room temperature and 77 K. Immediately apparent is the large difference between fluorescence and radiative lifetimes for both temperatures, which leads to low quantum efficiency values. This difference implies an efficient nonradiative process is depopulating the $^6H_{13/2}$ manifold. A likely candidate would be multiphonon relaxation; however, the temperature-dependent lifetime behavior presented in Fig. 9, showing a leveling off at low temperatures, implies that this process should be decreasing in magnitude as the phonons are frozen out. It is possible that other nonradiative processes could be

affecting this transition behavior, such as cross-relaxation processes, energy transfer between RE ions, or energy transfer to other defects in the crystal.

Note that the radiative lifetime should inherently be independent of temperature; and the fact that these values, as determined independently from the room temperature and 77-K data, are so similar is encouraging. Additionally, the radiative lifetime values calculated for Dy^{3+}-doped BaF_2 are comparable to those published for BaY_2F_8, another low maximum phonon energy fluoride.[20]

Table 2 Lifetime values of the $^6H_{13/2}$ manifold and quantum efficiency of the $^6H_{13/2} \rightarrow {}^6H_{15/2}$ transition for room temperature and 77 K

Temperature (K)	Fluorescence lifetime (ms)	Radiative lifetime (ms)	Quantum efficiency (%)
300	1.56	45.9	3.4
77	5.26	45.7	11.5

3.6 Gain Cross Sections

Gain cross section σ_g is a useful parameter for predicting the operation wavelength of a laser. The gain cross section is calculated from the absorption and stimulated emission cross sections using the following relationship:

$$\sigma_g(\lambda) = \beta\sigma_{se}(\lambda) - (1-\beta)\sigma_{abs}(\lambda) \quad (4)$$

where β is the population inversion parameter defined as the ratio of active ions in the excited state to the total number of active ions.[22] In general, lasing can occur when the gain cross section achieves a positive value. The calculated gain cross section spectra for a number of values of β are presented in Fig. 11 for room temperature and 77 K. From Fig 11a, it can be seen that a population inversion between 20% and 40% is needed to achieve positive gain for a broad wavelength region between 2900 and 3200 nm. Positive gain at the peak wavelength of 2847 nm requires an inversion of about 50%. A positive gain cross section is easier to achieve at 77 K, as can be seen in Fig. 11b. For this temperature, positive gain is achieved by 20% inversion with a clearly defined peak at 2925 nm.

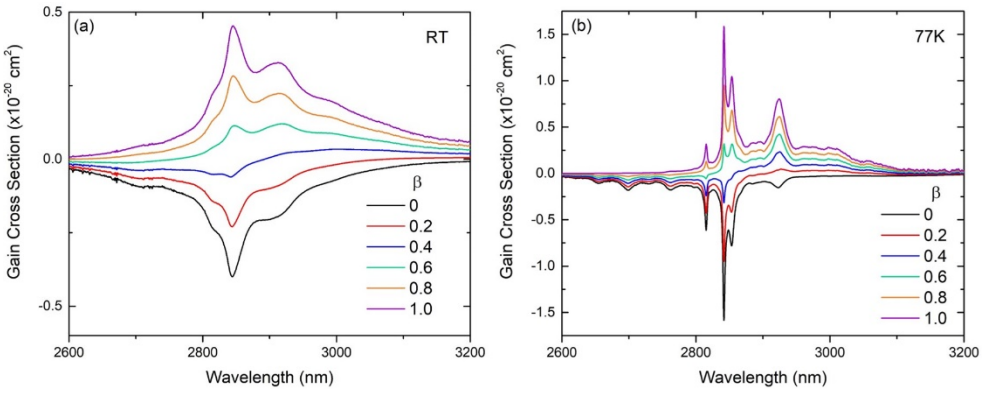

Fig. 11 Gain cross section at a) room temperature and b) 77 K for the 2.8-µm transition of Dy^{3+}:BaF_2 calculated for a number of different population inversion ratios β

4. Conclusions

In summary, comprehensive spectroscopic characterization relevant to the 2.8-µm emission was performed on Dy^{3+}-doped into the low maximum phonon crystal host BaF_2. Laser-relevant parameters including absorption and stimulated emission cross section, radiative lifetime, quantum efficiency, and gain cross section were determined for both room temperature and cryogenic temperature (77 K). Room-temperature laser operation of this transition would suffer from low quantum efficiency and would require a high population inversion of approximately 40%. The parameters at 77 K show improvement across the board with multiple-times-higher cross-section intensities, nearly 4× higher quantum efficiency, and a positive gain cross section requiring less than 20% population inversion.

Efforts to determine the discrete Stark splittings of various Dy^{3+} manifolds in this host material were hampered by apparent multisite behavior of the RE dopant. Multiple incorporation sites might be a side effect of the charge mismatch between the dysprosium and the barium ion that the dopant typically replaces in the crystal lattice. The multiple sites could be a factor in the rampant nonradiative decay prevalent in this transition. Future work might involve site-selective spectroscopic measurements that could shed light on this material system.

5. References

1. Taczak TM, Killinger DK. Development of a tunable, narrow-linewidth, CW 2.066-μm Ho:YLF laser for remote sensing of atmospheric CO_2 and H_2O. Appl Opt. 1998;37(36):8460.
2. Serebryakov VA, Boiko EV, Petrishchev NN, Yan AV. Medical applications of mid-IR lasers: problems and prospects. J Opt Technol. 2010;77(1):6.
3. Ishii S, Mizutani K, Fukuoka H, Ishikawa T, Philippe B, Iwai H, Aoki T, Itabe T, Sato A, Asai K. Coherent 2 micron differential absorption and wind lidar with conductively cooled laser and two-axis scanning device. Appl Opt. 2010;49(10):1809.
4. Eichhorn M**.** Quasi-three-level solid-state lasers in the near and mid infrared based on trivalent rare earth ions. Appl Phys. 2008;B(93):269.
5. Tittel FK, Richter D, Fried A. Mid-infrared laser applications in spectroscopy, solid-state mid-infrared laser sources. Topics Appl Phys. 2003;89:445.
6. Seddon AB, Tang Z, Furniss D, Sujecki S, Benson TM. Progress in rare-earth doped mid-IR fiber lasers. Opt Exp. 2010;18:26704.
7. Payne SA, Smith LK, Krupke WF. Cross sections and quantum yields of the 3 μm emission for Er3+ and Ho3+ dopants in crystals. J Appl Phys. 1995;77:4274.
8. Fleischman ZD, Sanamyan T. Spectroscopic analysis of Er3+:Y2O3 relevant to 2.7μm mid-IR laser. Opt Mat Exp. 2016;6(10):3109.
9. Brasse G, Doualan J-L, Benayad A, Braud A, Camy P. Dy3+ doped CaF2 crystals spectroscopy for the development of mid-infrared lasers around 3 μm. Proceedings of SPIE. 2018;10683(1068329).
10. Majewski MR, Woodward RI, Jackson SD. Dysprosium mid-IR lasers: current status and future prospects. Laser Photonics Rev. 2020;14:1900195.
11. Velazquez M, Ferrier A, Doualan J-L, Moncorge R. Rare-earth doped low phonon energy halide crystals for mid-IR sources. In: Al-Khursan A, editor. Solid-state laser. InTech online; 2012. p. 119–142.
12. Isaenko L, Yelisseyev A, Tkachuk A, Ivanova S. New monocrystals with low phonon energy for mid-IR lasers. In: Ebrahim-Zadeh M, Sorokinda IT, editors. Mid-infrared coherent sources and applications. Berlin (Germany): Springer; 2008. p. 3–65.

13. Labbe C, Doualan JL, Camy P, Moncorge R, Thuau M. The 2.8 μm laser properties of Er^{3+} doped CaF_2 crystals. Opt Comm. 2002;209:193.

14. Svejkar R, Sulc J, Jelinkova H, Kubecek V, Ma W, Jiang D, Wu Q, Su L. Diode-pumped Er:SrF_2 laser tunable at 2.7 μm. Opt Mater Exp. 2018;8:1025.

15. Nara H, Schlesinger M. Analysis of the optical spectra of Dy3 + doped calcium fluoride. J Phys C Solid State Phys. 1972;5:606.

16. Jamison SP, Reeves RJ. Site-selective laser and Zeeman infrared spectroscopy of Dy3+ centers in SrF2:Dy3+. Phys Rev B. 2003;67:115110.

17. Bitam A, Khiari S, Diaf M, Boubekri H, Boulma E, Bensalem C, Guerbous L, Jouart JP. Spectroscopic investigation of Er^{3+} doped BaF_2 single crystal. Opt Mater. 2018;82:104.

18. Richman I. Longitudinal optical phonons in CaF2, SrF2, and BaF2. J Chem Phys. 1964;41:2836.

19. Zhang L, Zhang J, Yu C, Hu L. A method for emission cross section determination for Tm^{3+} at 2.0 μm emission. J Appl Phys. 2010;108:103117.

20. Toncelli A, Tonelli M, Cassanho A, Jenssen HP. Spectroscopy and dynamic measurements of a Tm,Dy:BaY2F8 crystal. J Lumin. 1999;92:291.

21. Aull BF, Jenssen HP. Vibronic interactions in Nd:YAG resulting in nonreciprocity of absorption and stimulated emission cross sections. IEEE Quantum Electron. 1982;18:925–930.

22. Ryba-Romanowski W. YVO4 crystals – puzzles and challenges. Cryst Res Technol. 2003;38(35):225.

List of Symbols, Abbreviations, and Acronyms

BaF_2	barium fluoride
CaF_2	calcium fluoride
Dy^3	dysprosium
Er^{3+}	erbium
F-L	Fuchtbauer–Ladenburg
Ho^{3+}	holmium
InSb	indium antimonide
IR	infrared
lidar	light detection and ranging
MPR	multiphonon relaxation
Nd:YAG	neodymium:yttrium aluminum garnet
RE	rare earth
SrF_2	strontium fluoride
Ti	titanium

1 (PDF)	DEFENSE TECHNICAL INFORMATION CTR DTIC OCA
1 (PDF)	CCDC ARL FCDD RLD DCI TECH LIB
4 (PDF)	CCDC ARL FCDD RLS RL Z FLEISCHMAN J ROSEN E E BROWN M DUBINSKII